Available online at www.sciencedirect.com
ScienceDirect
Journal of Molecular Structure 881 (2008) 28–45
Journal of MOLECULAR STRUCTURE
www.elsevier.com/locate/molstruc

Preparation, structural characterization and biological evaluation of L-tyrosinate metal ion complexes

Moamen S. Refat [a,*], Sabry A. El-Korashy [b], Ahmed S. Ahmed [a]

[a] Department of Chemistry, Faculty of Education, Port Said, Suez Canal University, Mohamed Ali Street, Port Said, Egypt
[b] Department of Chemistry, Faculty of Science, Ismalia, Suez Canal University, Ismalia, Egypt

Received 18 April 2007; received in revised form 17 August 2007; accepted 20 August 2007
Available online 4 September 2007

Abstract

The complexes formed between different metal ions and biological molecules like amino acids play an important role in human life. Sn(II), Sn(IV), Zn(II), Cd(II), Hg(II), Cr(III), Fe(III), La(III), ZrO(II) and UO_2(II) complexes are synthesized with L-tyrosine (tyr). These complexes are characterized by elemental analysis, molar conductance, magnetic measurements, mass, IR, UV–vis and ^{1}H NMR spectra as well as thermogravimetric analysis (TGA/DTG). It has been found from the elemental analysis and the thermal studies that the ligand behaves as bidentate ligand forming chelates with 1:3 (metal:ligand) stoichiometry for trivalent metals and 1:2 for divalent and tetravalent metals. The molar conductance measurements of the complexes in DMSO indicate that the complexes are non-electrolyte. The activation energies and other kinetic parameters were calculated from the Coats–Redfern and Horowitz–Metzger equations. The biological activities of the metal complexes have also been studied against different bacteria and fungi.

Keywords: L-Tyrosine; Microbiological investigation; Infrared spectra; Thermogravimetric analyses

1. Introduction

Amino acids and their compounds with different metal ions play an important role in biology, pharmacy and industry [1]. Tyrosine (Tyr), 2-amino-3-(4-hydroxyphenyl)-propanoic, H_2L, is non-essential amino acid for human development and precursor for the synthesis of thyroid hormones and select neurotransmitters, such as dopamine and norepinephrine, may be considered essential by the brain [2]. In plants, solar energy is used to extract electrons from water, producing atmospheric oxygen. This is conducted by Photosystem, where a redox ''triad'' consisting of chlorophyll, a tyrosine, and a manganese cluster, governs an essential part of the process [3].

A review of the literature on tyrosine suggests that the phenolic oxygen does not participate in coordination reaction to metal ions with the result that formation constants are close to those of phenyl alanine itself. However, this oxygen does appear to coordinate to Cu(II) in some dipeptide complexes [4] and X-ray analysis of [Cu(L-tyr)$_2$] [L-tyr = L-tyrosinate (1−)] shows an abnormally short Cu-phenyl ring distance [5].

For a number of metalloproteins of biological importance it assumed [6] that the phenolate oxygen in tyrosine acts as a metal ion binding site. Extensive investigations have therefore been made to establish the complex-forming properties of transition metal ions with tyrosine, with special regard to the participation of phenolate group in complex formation [7]. The phenolic hydroxyl group in *o*-tyrosine is in a sterically more favorable position for coordination to the metal ion in its complexes. Letter and Bauman [8] made a comparative study of the copper(II) complexes of tyrosine, *m*-tyrosine, and *o*-tyrosine (4-, 3-, and 2-hydroxyphenylalanine, respectively; H_2A). From the absorption band at 390 nm, indicative of the copper(II)-phenolate interaction for *o*-tyrosine, they assumed direct coordination of the phenolate oxygen at pH 10.

* Corresponding author.
E-mail address: msrefat@yahoo.com (M.S. Refat).

0022-2860/$ - see front matter © 2007 Elsevier B.V. All rights reserved.
doi:10.1016/j.molstruc.2007.08.027

The coordinate of L-tyrosine with rare earth element Eu^{3+} was investigated in solution by ultraviolet and was proved the molar ratio was 1:2, and then the solid complex was prepared by coprecipitation method [9].

Schiff bases derived from L-tyrosine and their metal complexes have wide application in biological science, like, $ML_2[H_2O]_2$ where (M = Mn, Co, Ni and Cu) were synthesized and were screened for their antifungal behavior against Phytophthora capsici, the casual organism of foot rot of black pepper [10]. A convenient method for the preparation of transition metal complexes of L-tyrosine was reported and this had enabled eight complexes of tyrosinate anion (tyr) to be prepared: $[M(tyr)_2(H_2O)_n]$ (M = Co, Ni, Cu, Zn; $n = 1, 2, 3$), $[Cu(tyr)(NO_3)]$, and $Li[Cu(tyr)_3]$ [11,12]. In view of the literature, the coordination chemistry of tyrosine with heavy metals is obscure. In the paper herein, we report the formation of 10 new amino acid complexes obtained from the reaction of L-tyrosine with the 10 metal ions in aqueous media.

The aim of this study is to make an assessment of the coordination behavior of the resulting new complexes formed.

2. Experimental

2.1. Materials

L-Tyrosine (BDH), $SnCl_2$, $SnCl_4$, $ZnBr_2$, $CdCl_2$, $HgCl_2$, $CrCl_3{\cdot}6H_2O$, $FeCl_3$, $La(NO_3)_3{\cdot}6H_2O$, $ZrOCl_2{\cdot}6H_2O$, $UO_2(NO_3)_2{\cdot}6H_2O$ and $LiOH{\cdot}H_2O$ (Merck) were purchased and used without further purification.

2.2. Synthesis of metal complexes

First experiments were performed in order to find, if possible, a general method for the preparation of L-tyrosine complexes. Many amino acids will react with metal ions in aqueous solutions, but reaction appeared to occur between solutions of L-tyrosine and metal salts in water, at room temperature or at 70 °C.

It was found that lithium hydroxide powder was preferable to sodium hydroxide or potassium hydroxide pellets, as more accurate weight is possible with the powder.

A second approach was via the reaction of L-tyrosine with lithium hydroxide in water at room temperature; subsequent addition of aqueous metal salt solutions did not appear to lead to complex formation. However, it was found that by heating the tyrH-$LiOH{\cdot}H_2O$ solution to 70 °C for 20 min, followed by addition of the metal salts, complexes formed readily.

2.2.1. $[Sn(tyr)_2]{\cdot}H_2O$ (**I**, $C_{18}H_{22}N_2O_7Sn$)

L-Tyrosine (0.543 g, 3.0 mmol) and $LiOH{\cdot}H_2O$ (0.126 g, 3.0 mmol) were dissolved in water (25 ml) and the solution heated to 70 °C for 20 min. The $SnCl_2{\cdot}2H_2O$ salt (0.433 g, 1.5 mmol) was dissolved in a minimum quantity of water and the solutions mixed with vigorous stirring (for a 1:2 metal:ligand ratio), the metal salt was added to the tyrH-$LiOH{\cdot}H_2O$ solution. Precipitation was almost instantaneous, but stirring with heating were continued for 15 min. The Sn(II) complex was filtered, washed with hot water (25 ml), and dried *in vacuo* over anhydrous $CaCl_2$.

2.2.2. $[Sn(tyr)_2(Cl)_2]$ (**II**, $C_{18}H_{20}N_2O_6SnCl_2$)

A similar procedure as that described for complex **I** was carried out, but the weights of L-tyrosine (0.724 g, 4.0 mmol), $LiOH{\cdot}H_2O$ (0.168 g, 4.0 mmol) and $SnCl_4{\cdot}5H_2O$ was 0.350 g and 1.0 mmol.

2.2.3. $[Zn(tyr)_2]{\cdot}2H_2O$ (**III**, $C_{18}H_{24}N_2O_8Zn$)

L-Tyrosine (0.543 g, 3.0 mmol) and $LiOH{\cdot}H_2O$ (0.126 g, 3.0 mmol) were dissolved in water (25 ml) and the solution heated to 70 °C for 20 min. The $ZnBr_2$ salt (0.337 g, 1.5 mmol) was dissolved in a minimum quantity of water and the solutions mixed with vigorous stirring (for a 1:2 metal:ligand ratio), the metal salt was added to the tyrH-$LiOH{\cdot}H_2O$ solution. Precipitation was almost instantaneous, but stirring with heating were continued for 15 min. The Zn(II) complex was filtered, washed with hot water (25 ml), and dried *in vacuo* over anhydrous $CaCl_2$.

2.2.4. $[Cd(tyr)_2]{\cdot}2H_2O$ (**IV**, $C_{18}H_{24}N_2O_8Cd$)

A similar procedure as that described for complex **III** was carried out the weight of $CdCl_2$ was 0.302 g and 1.5 mmol.

2.2.5. $[Hg(tyr)_2]$ (**V**, $C_{18}H_{20}N_2O_6Hg$)

A pale brown compound was prepared by the same method as under compound **III**. The weight of $HgCl_2$ was 0.407 g and 1.5 mmol.

2.2.6. $[Cr(tyr)_3]{\cdot}6H_2O$ (**VI**, $C_{27}H_{42}N_3O_{15}Cr$)

L-Tyrosine (0.543 g, 3.0 mmol) and $LiOH{\cdot}H_2O$ (0.126 g, 3.0 mmol) were dissolved in water (25 ml) and the solution heated to 70 °C for 20 min. The $CrCl_3{\cdot}6H_2O$ salt (0.286 g, 1.0 mmol) was dissolved in a minimum quantity of water and the solutions mixed with vigorous stirring (for a 1:3 metal:ligand ratio), the metal salt was added to the tyrH-$LiOH{\cdot}H_2O$ solution. Precipitation was almost instantaneous, but stirring with heating were continued for 15 min. The Cr(III) complex was filtered, washed with hot water (25 ml), and dried in vacuo over anhydrous $CaCl_2$.

2.2.7. $[Fe(tyr)_3]$ (**VII**, $C_{27}H_{30}N_3O_9Fe$)

Exactly like the above procedure of the Cr(III) complex preparation but the weight of $FeCl_3$ was 0.162 g and 1.0 mmol.

2.2.8. $[La(tyr)_3]{\cdot}7H_2O$ (**VIII**, $C_{27}H_{44}N_3O_{16}La$)

Preparation of this compound followed essentially the same procedure as preparation of **VI**, but the weight of $La(NO_3)_3{\cdot}6H_2O$ was 0.433 g and 1.0 mmol.

*2.2.9. $[ZrO(tyr)_2]\cdot 2H_2O$ (**IX**, $C_{18}H_{24}N_2O_9Zr$)*

L-Tyrosine (0.543 g, 3.0 mmol) and $LiOH\cdot H_2O$ (0.126 g, 3.0 mmol) were dissolved in water (25 ml) and the solution heated to 70 °C for 20 min. The $ZrOCl_2\cdot 6H_2O$ salt (0.429 g, 1.5 mmol) was dissolved in a minimum quantity of water and the solutions mixed with vigorous stirring (for a 1:2 metal:ligand ratio), the metal salt was added to the tyrH-$LiOH\cdot H_2O$ solution. Precipitation was almost instantaneous, but stirring with heating were continued for 15 min. The ZrO(II) complex was filtered, washed with hot water (25 ml), and dried *in vacuo* over anhydrous $CaCl_2$.

*2.2.10. $[UO_2(tyr)_2]$ (**X**, $C_{18}H_{20}N_2O_8U$)*

Exactly like the above procedure of the ZrO(II) complex preparation but the weight of $UO_2(NO_3)_2\cdot 6H_2O$ was 0.753 g and 1.5 mmol.

2.3. Apparatus and experimental conditions

2.3.1. Elemental analysis and metal percentage

Elemental analyses (C, H, and N) were performed using a Perkin-Elmer CHN 2400 elemental analyzer. The percentages of the metal ions of the complexes were determined gravimetrically by converting the compounds into their corresponding oxides.

2.3.2. Molar conductance

Molar conductance measurements of the L-tyr ligand and their complexes with 1.0×10^{-3} mol/l in DMSO were carried out using Jenway 4010 conductivity meter.

2.3.3. Magnetic measurements

Magnetic measurements were carried out on a Sherwood Scientific magnetic balance in the micro analytical laboratory using Gouy method.

Calibration: Two very good solid calibrants are $Hg[Co(CNS)_4]$ and $[Ni(en)_3](S_2O_3)$. They are easily prepared pure, do not decompose or absorb moisture and pack well. Their susceptibilities at 20 °C are 16.44×10^{-6} and 11.03×10^{-6} c.g.s. Units, decreasing by 0.05×10^{-6} and 0.04×10^{-6} per degree temperature raise, respectively, near room temperature. The cobalt compound, besides having the higher susceptibility, also packs rather densely and is suitable for calibrating low fields, while the nickel compound with lower susceptibility and density is suitable for higher field [13]. Here we are used $Hg[Co(CNS)_4]$ only as calibrant.

2.3.4. Infrared spectra

IR spectra (4000–400 cm^{-1}) were recorded as KBr pellets on Bruker FT-IR Spectrophotometer.

2.3.5. Electronic spectra

The UV–vis, Spectra were obtained for the DMSO solution (1.0×10^{-3} M) of the L-tyr and their 10 complexes with a Jenway 6405 Spectrophotometer using 1 cm quartz cell, in the range 200–550 nm.

2.3.6. ^1H NMR spectra

The structures of L-tyrosine, Sn(IV), Hg(II), Cr(III) and ZrO(II) complexes were elucidated using a Varian Gemini 200 MHz ^1H NMR spectrometer. The L-tyrosine and the above complexes were added into sample tubes and dissolved in DMSO-d_6 and TMS as an internal reference. The ^1H NMR was done at 25 °C.

2.3.7. Mass spectra

The purity of the Sn(II), Zn(II), Fe(III) and UO_2(II) complex were checked from mass spectra at 70 eV by using AEI MS 30 Mass spectrometer.

2.3.8. Thermal analysis (TG) and (DTG) techniques

Thermogravimetric analyses (TG) were carried out in the temperature range from 25 to 800 °C in a steam of nitrogen atmosphere by Shimadzu TGA 50H thermal analysis. The experimental conditions were: platinum crucible, nitrogen atmosphere with a 30 ml/min flow rate and a heating rate 10 °C/min.

2.3.9. Microbiological investigation

For these investigations the filter paper disc method was applied. The investigated isolates of bacteria were seeded in tubes with nutrient broth (NB). The seeded NB (1 cm^3) was homogenized in the tubes with 9 cm^3 of melted (45 °C) nutrient agar (NA). The homogeneous suspensions were poured into Petri dishes. The discs of filter paper (diameter 4 mm) were ranged on the cool medium. After cooling on the formed solid medium, 2×10^{-5} dm^3 of the investigated compounds were applied using a micropipette. After incubation for 24 h in a thermostat at 25–27 °C, the inhibition (sterile) zone diameters (including disc) were measured and expressed mm. An inhibition zone diameter over 7 mm indicates that the tested compound is active against the bacteria under investigation.

The antibacterial activities of the investigated compounds were tested against *Escherichia coli*, *Bacillus subtilis*, *Serratia* and *Pseudomonas aeruginosa* as well as some kinds of fungi; *Aspergillus flavus*, *Fusarium solani* and *Penicillium verrucosum*. The concentration of each solution was 1.0×10^{-3} mol dm^3. Commercial DMSO was employed to dissolve the tested samples.

3. Results and discussion

Ten, L-tyrosine complexes (Sn(II) and Sn(IV)), (Zn(II), Cd(II) and Hg(II)), (Cr(III), Fe(III) and La(III)) and (ZrO(II) and UO_2(II)) rather L-tyrosine ligand have been synthesized according to the following synthetic method:

For,

(i) Sn(II) complex, (**I**)

$$SnCl_2 + 2[tyrH\text{-}LiOH\cdot H_2O] \xrightarrow{\text{aqueous media}} [Sn(tyr)_2]\cdot H_2O$$

(ii) Sn(IV) complex, (**II**)

$$SnCl_4 + 4[tyrH\text{-}LiOH \cdot H_2O] \xrightarrow{\text{aqueous media}} [Sn(tyr)_2Cl_2]$$

(iii) Zn(II) complex, (**III**)

$$ZnBr_2 + 2[tyrH\text{-}LiOH \cdot H_2O] \xrightarrow{\text{aqueous media}} [Zn(tyr)_2] \cdot 2H_2O$$

(iv) Cd(II) complex, (**IV**)

$$CdCl_2 + 2[tyrH\text{-}LiOH \cdot H_2O] \xrightarrow{\text{aqueous media}} [Cd(tyr)_2] \cdot 2H_2O$$

(v) Hg(II) complex, (**V**)

$$HgCl_2 + 2[tyrH\text{-}LiOH \cdot H_2O \xrightarrow{\text{aqueous media}} [Hg(tyr)_2]$$

(vi) Cr(III) complex, (**VI**)

$$CrCl_3 + 3[tyrH\text{-}LiOH \cdot H_2O] \xrightarrow{\text{aqueous media}} [Cr(tyr)_3] \cdot 6H_2O$$

(vii) Fe(III) complex, (**VII**)

$$FeCl_3 + 3[tyrH\text{-}LiOH \cdot H_2O] \xrightarrow{\text{aqueous media}} [Fe(tyr)_2]$$

(viii) La(III) complex, (**VIII**)

$$La(NO_3)_2 + 3[tyrH\text{-}LiOH \cdot H_2O] \xrightarrow{\text{aqueous media}} [La(tyr)_3] \cdot 7H_2O$$

(ix) ZrO(II) complex, (**IX**)

$$ZrOCl_2 + 2[tyrH\text{-}LiOH \cdot H_2O] \xrightarrow{\text{aqueous media}} [ZrO(tyr)_2 \cdot 2H_2O$$

(x) UO_2(II) complex, (**X**)

$$UO_2Cl_2 + 2[tyrH\text{-}LiOH \cdot H_2O] \xrightarrow{\text{aqueous media}} [UO_2(tyr)_2]$$

The L-tyrosine complexes were investigated in this study, are very stable at room temperature in the solid state. These complexes; Sn(II), Sn(IV), Zn(II), Cd(II), Hg(II), Cr(III), Fe(III), La(III), ZrO(II) and UO_2(II) are insoluble in common organic solvents in cold or hot conditions except DMSO (dimethylsulphoxide).

No suitable crystals of the complexes were obtained in order to perform an X-ray structure determination. The physical properties: colors, melting and/or decomposition points, elemental analyses and molar conductance of the free ligand and its complexes are given in Table 1. The analytical data are in a good agreement with the proposed stoichiometry of the complexes.

The metal-to-ligand ratio in Sn(II), Sn(IV), Zn(II), Cd(II), Hg(II), ZrO(II) and UO_2(II) complexes were the same molar ratio, that found to be 1:2 (metal:ligand) but these are different in the coordination behaviors. On the other hand, the Cr(III), Fe(III) and La(III) tyrosine complexes have been coordinated to (1:3) molar ratio.

3.1. Elemental analysis data

The elemental analysis measurements of the carbon, nitrogen, hydrogen, and the percentage of metal ions for the synthesized complexes are illustrated in Table 1.

3.2. Molar conductivities of metal chelates

Conductivity measurements in non-aqueous solutions have frequently been used in structural studies of metal chelates within the limits of their solubility. They provide a method of testing the degree of ionization of the complexes, the molar ions that a complex liberates in solution, the higher will be its molar conductivity and vice versa. The non-ionized complexes have negligible value of molar conductance. The molar conductivities of the solid chelates are measured for 1.0×10^{-3} mol solution of 1:2 and 1:3 complexes in DMSO. The conductivity data reported for these complexes are given in Table 1. It is clear from the conductivity data that the complexes present behave as non-electrolytes [14] behavior. The molar conductivity values for all the complexes in organic solvent (DMSO) with 10^{-3} mol were in rang of (11.7–19.2) $\Omega^{-1}\,cm^{-1}\,mol^{-1}$ (Table 1).

3.3. Magnetic measurements

Magnetic measurements were carried out on a Sherwood Scientific magnetic balance according to the Gauy method.

The magnetic moments of the Cr(III) and Fe(III) complexes at $T = 300$ K and their corresponding hybrid orbitals are given in Table 2. From the data given in Table 2, the observed values of the effective magnetic moments μ_{eff} measured for the $[Cr(tyr)_3]\cdot 6H_2O$ and $[Fe(tyr)_3]$ complexes equal to 3.13 and 2.18 B.M., respectively, this is in convenient with experimental values of 3.77 and 2.25 B.M. [13] obtained for high spin octahedral Cr(III) complex and low spin octahedral Fe(III) complex, with hyperdization of d^2sp^3 for both complexes.

3.4. Infrared spectra

The IR spectra in the (4000–400 cm^{-1}) region have provided information regarding the coordination mode in the L-tyrosine complexes and were analyzed by comparison with data for the free L-tyrosine ligand. The most relevant bands and proposed assignments for all the complexes are mentioned in Table 3. In the FT-IR spectra, extensive coupling occurs for several vibrations, making qualitative deductions about the environment around metal ions difficult. However, the IR spectral data (Table 3) shown changes in the position and profiles of some bands, as compared to those of free L-tyrosine (amino acid), suggesting participation of the groups that produce these bounds in the coordination with metal ions Sn(II), Sn(IV), Zn(II), Cd(II), Hg(II), Cr(III), Fe(III), La(III), ZrO(II) and UO_2(II). Major changes are related to the carboxylate and amine bands.

(i) Ligand (L-tyr); amino acid physical properties indicate a "salt-like" behavior. Amino acids are crystalline solids with relatively high melting points, and

Table 1
Elemental analyses and physical data of the tyrosine complexes

Compounds	Mwt.	Mp (°C) or decomp.	Color	Content ((calculated) found)				Λm (Ω^{-1} cm^{-1} mol^{-1})
				% C	% H	% N	%M	
L-Tyrosine ($C_9H_{11}NO_3$)	181.19	344 dec.	White	59.66 (59.60)	6.12 (6.07)	7.73 (7.59)	–	11.7
$[Sn(tyr)_2]\cdot H_2O$ (**I**, $C_{18}H_{22}N_2O_7Sn$)	496.69	275 dec.	White	43.38 (43.49)	4.41 (4.43)	5.33 (5.64)	23.73 (23.92)	14.02
$[Sn(tyr)_2(Cl)_2]$ (**II**, $C_{18}H_{20}N_2O_6SnCl_2$)	549.69	280	White	38.98 (39.29)	3.57 (3.64)	5.07 (5.09)	21.40 (21.59)	19.2
$[Zn(tyr)_2]\cdot 2H_2O$ (**III**, $C_{18}H_{24}N_2O_8Zn$)	461.38	290 dec.	Pale Yellow	46.77 (46.82)	5.13 (5.20)	5.68 (6.07)	13.93 (14.17)	11.98
$[Cd(tyr)_2]\cdot 2H_2O$ (**IV**, $C_{18}H_{24}N_2O_8Cd$)	508.4	235	Pall Brown	42.31 (42.49)	4.67 (4.72)	4.85 (5.51)	22.07 (22.11)	13.07
$[Hg(tyr)_2]$ (**V**, $C_{18}H_{20}N_2O_6Hg$)	560.59	320 dec.	Pall Brown	38.53 (38.20)	3.56 (3.57)	4.99 (5.12)	(35.78) (35.18)	11.78
$[Cr(tyr)_3].6H_2O$ (**VI**, $C_{27}H_{42}N_3O_{15}Cr$)	699.99	275 dec.	Green	45.89 (46.28)	5.91 (6.00)	5.71 (6.00)	7.39 (7.43)	13.84
$[Fe(tyr)_3]$ (**VII**, $C_{27}H_{30}N_3O_9Fe$)	595.84	270	Brown	54.31 (54.38)	4.99 (5.03)	6.81 (7.05)	9.28 (9.37)	12.41
$[La(tyr)_3]\cdot 7H_2O$ (**VIII**, $C_{27}H_{44}N_3O_{16}La$)	804.91	270 dec.	Pall Brown	39.87 (40.25)	(5.93) (5.47)	4.72 (5.22)	17.18 (17.26)	18.70
$[ZrO(tyr)_2]\cdot 2H_2O$ (**IX**, $C_{18}H_{24}N_2O_9Zr$)	503.22	240 dec.	White	(42.98) (42.52)	4.29 (4.74)	5.43 (5.33)	18.13 (18.23)	16.14
$[UO_2(tyr)_2]$ (**X**, $C_{18}H_{20}N_2O_9U$)	630.03	270	Yellow	34.19 (34.28)	3.09 (3.17)	4.37 (4.44)	37.70 (37.78)	13.62

Table 2
The magnetic moment of the Cr(III) and Fe(III) complexes

Complex	μ_{eff} B.M. (found)	μ_{eff} B.M. (calcd.)	Hybrid orbitals	Stereo-chemistry
$[Cr(tyr)_3]\cdot 6H_2O$	3.13	3.77	d^2sp^3	Octahedral
$[Fe(tyr)_3]$	2.18	2.25	d^2sp^3	Octahedral

almost are quite soluble in water and insoluble in non-polar solvents. In solution, the amino acid molecule appears to have a change which changes with pH. As intermolecular neutralization reaction leads to a salt-like ion called a Zwitterion. The accepted practice is to show the amino acids in the Zwitterion from (Scheme 1); (i) the amino group can lose a

Table 3
Important FT-IR bands of the L-tyrosine and its metal complexes

Assignments (cm^{-1})	Compound										
	L-Tyr	**I**	**II**	**III**	**IV**	**V**	**VI**	**VII**	**VIII**	**IX**	**X**
NH_2 asym. str.	–	3375	3390	3364	3382	3322	3420	3422	3378	3399	3423
NH_2 sym. str.				3307 3270	3262	3273					
NH_3 str.	3124	3206	3206	3178	3204	3120	3206	3206	3205	3206	3207
OH str.	3205										
COO^- asym.	1612	1610	1610	1615	1610	1578	1610	1610	1611	1611	1609
δNH_2	1588	1588	1587	1544	1588		1589	1589	1588	1588	1589
COO^- sym.	1416	1416	1416	1399	1407	1424	1416	1416	1415	1416	1416
δCH; CH_2	1364	1364	1364		1369	1367	1365	1364	1364	1364	1364
OH in plane def.	1243	1245	1245	1234	1243	1252	1246	1246	1244	1244	1247
NH_2 wagging	–	1042	1042	–	1044	1069 1043	1041	1042	1042	1042	1042
OH out of plane def.	648	649	649	658	649	679	648	649	649	650	650
NH_2 rocking	–	575	575	543	574	595 569	574	575	575	576	575
M-N str.	–	432	432	420	432	420	418	432	432	433	434

hydrogen ion to become negative charged, (ii) the amino group can accept a hydrogen ion to become positive charged.

(ii) Assignment of observed frequencies; in all spectra, the characteristic band of NH_2 group vibration appears at ~3300 and ~3400 cm^{-1} corresponding to $v_s(NH_2)$ and $v_{as}(NH_2)$, respectively. In the spectra of complex compounds, this band overlap with the well defined very intense due to the hydrogen bond of crystalline water.The band due to the NH_3^+ group $v(NH_3^+)$ at ~3124, 2950 and 2500 cm^{-1} [15], which are very intense in the free ligand, appears as a weak shoulder or disappear in the spectra of the complex compounds.The sharp band at around 3200 cm^{-1} is assigned to the OH stretching vibration; the broad bands from 3100 to 2800 cm^{-1} are due to NH_3^+ and CH stretching vibrations of the benzene ring. The CH stretching vibrations of an aliphatic group are observed in a lower frequency region than those of a benzene ring.

(iii) Metal-chelates; in all of the complexes it is apparent that the tyrosine moiety complexes as the tyrosinate anion [9,11,16,17]. Tyrosine can lose a proton in two ways: from the carboxylic acid group or from the phenolic group. It is to be expected that carboxylic acid group will deprotonated preferentially, especially the α-amino acid moiety acts as a chelate. In the present study no specific attempt was made to deprotonate the phenolic (hydrogen) and there is no evidence to suggest that it occurred in advertently.

As the bands above 3500 cm^{-1} of the Sn(II), Zn(II), Cd(II), Cr(III), La(III) and ZrO(II) chelates disappear in the IR spectra, are obtained often TGA analysis, these bands are assigned to the OH stretching vibrations in the water of crystallization.

Although the bands from 3400 to 3100 cm^{-1} are due to NH_2 symmetric and asymmetric and OH stretching vibrations are observed at the same region as in the ligand.

In the region 1700–500 cm^{-1} the assignments of the observed bands is accomplished by a comparison of the spectrum of each chelate with that of the L-tyrosine free ligand. For the metal chelates, the NH_2 deformation vibrations appear in stead of NH_3^+ deformation vibrations of the ligand. The $v(COO^-)$ antisymmetric stretching vibrations of the benzene ring and the $\delta(NH_2)$ vibrations to some extent. The $v(COO^-)$ antisymmetric stretching are observed at the same frequencies and symmetric stretching vibrations are at the same region frequencies (with varying in the intensity of bands) than those of the ligand in the Zwitterion feature.

The OH in plane and out of plane deformation vibrations has no detected frequencies. The vibrations of the phenolic group, the skeletal deformation vibrations occur at the same regions as in the ligand.

From 500 to 400 cm^{-1}, absorption bands which cannot be observed in the ligand or appear with shifted in frequencies or the intensities were defected dependently on the complexation. The absorption bands appear at 432 cm^{-1} for Sn(II), 432 cm^{-1} for Sn(IV), 420 cm^{-1} for Zn(II), 432 cm^{-1} for Cd(II), 420 cm^{-1} for Hg(II), 418 cm^{-1} for Cr(III), 432 cm^{-1} for Fe(III), 432 cm^{-1} for La(III), 433 cm^{-1} for ZrO(II) and 434 cm^{-1} for UO_2(II) complexes, respectively. They are assigned to the metal-nitrogen stretching vibration by comparison of the chelate spectra with the ligand spectrum and referring to the metal chelate amino acids [18–21].

For the L-tyrosine adducts, the observed $v_{as}(COO^-)$ band was exhibits at ~1610 cm^{-1} as well as the $v_s(COO^-)$ band which appears at ~1400 cm^{-1}, are in agreement with coordination involving the amine nitrogen, as well as an oxygen atom of the carboxylate group [22,23]. The Δv difference (asymmetric–symmetric) is ranged from 193 to 216 cm^{-1}, this value proved that, metal ions coordinated to carboxylate group of L-tyrosine ligand as a monodentate chelates [15].

The v(U=O) vibration in the uranyl complex is observed as expected as a medium strong at 930 cm^{-1} is a good agreement with those known for many dioxouranium (VI) complexes [24,25]. On the other hand, concerning, the infrared spectra of $[ZrO]^{2+}$ complex show a medium strong absorption band at 1040 account that v(Zr=O) as expected [26].

Account that tyrosine acts as a bidentate ligand, data about the complex compounds formation were obtained mainly by comparing the absorption bands due to the vibrations of NH_3^+ and COO^- groups.

3.5. Electronic spectra

The bands in the range 200–450 nm can be assigned to n–π^* and/or π–π^* intraligand transition associated to

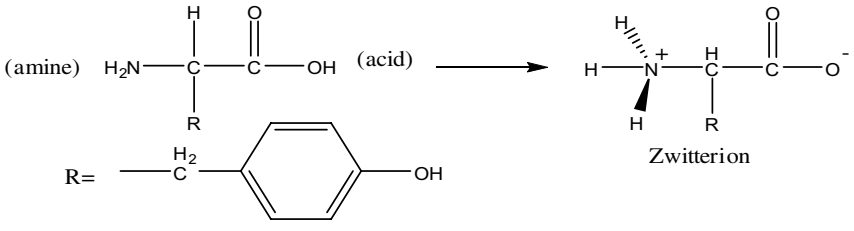

Scheme 1. Zwitterion structure of L-tyrosine.

amino acid (L-tyrosine). Free ligand and complexes exhibit similar spectra in UV region in relation to the number of the absorption peaks.

The electronic spectra of L-tyrosine and its complexes were recorded in DMSO and listed in Table 4.

The electronic absorption spectrum of the free ligand shows three absorption peaks appearing at $\lambda_{max} = 230$, 240 and 280 nm. The first two bands are attributed to the intraligand π–π^* transition [27], and the third can be attributed to the intraligand n–π^* charge transfers [28–30]. The electronic absorption spectra of the complexes are different from the spectrum of the free ligand, where there are forth bands appearing in the spectrum of Sn(II) complex. The first two band appeared at 220, 235 nm, which represent the intraligand π–π^* transition. The second two bands appeared at 245, 280 nm, which can be assigned to the intraligand n–π^* charge transfers. But in the spectra of Sn(IV) complex there are three bands only, the first two, which are appeared at 235, 250 nm represented the intraligand π–π^* transition, and the third, which at 275 nm, can be interpretated to the intraligand n–π^* charge transfers.

Table 4
The electronic spectral date of the free ligand and its complexes

Compound	λ_{max} (nm)	ε (mol^{-1} cm^{-1})	Assignment
L-Tyr	230	471	π–π^* trans.
	240	199	π–π^* trans.
	280	1189	n–π^* trans.
$[Sn(tyr)_2]\cdot H_2O$	220	265	π–π^* trans.
	235	155	π–π^* trans.
	245	370	n–π^* trans.
	280	1947	n–π^* trans.
$[Sn(tyr)_2(Cl)_2]$	235	211	π–π^* trans.
	250	3000	π–π^* trans.
	275	3000	n–π^* trans.
$[Zn(tyr)_2]\cdot 2H_2O$	220	270	π–π^* trans.
	235	1224	π–π^* trans.
	280	2943	n–π^* trans.
	325	500	L → Zn C.T.
$[Cd(tyr)_2]\cdot 2H_2O$	225	3000	π–π^* trans.
	245	3000	π–π^* trans.
	285	2919	n–π^* trans.
$[Hg(tyr)_2]$	220	1134	π–π^* trans.
	240	284	π–π^* trans.
	280	3000	n–π^* trans.
$[Cr(tyr)_3]\cdot 6H_2O$	220	330	π–π^* trans.
	275	1510	n–π^* trans.
	435	190	L → Cr C.T.
$[Fe(tyr)_3]$	245	673	π–π^* trans.
	270	2499	n–π^* trans.
	285	2552	n–π^* trans.
$[La(tyr)_3]\cdot 7H_2O$	225	192	π–π^* trans.
	245	246	π–π^* trans.
	270	2874	n–π^* trans.
	285	3000	n–π^* trans.
$[ZrO(tyr)_2]\cdot 2H_2O$	245	282	π–π^* trans.
	285	2628	n–π^* trans.
$[UO_2(tyr)_2]$	225	382	π–π^* trans.
	235	946	π–π^* trans.
	245	205	n–π^* trans.
	280	2427	n–π^* trans.
	400	300	L → UO_2 C.T.

The electronic absorption spectra of Zn(II) complex show four bands. The first two band appeared at 220, 235 nm, which represent the intraligand π–π^* transition. The third band appeared at 280 nm, which can be attributed to the intraligand n–π^* charge transfers. The forth band, which is abroad band, appeared at range 325 nm, can be assigned to L → Zn(II) charge transfers. But in the spectra of Cd(II) and Hg(II) complex there are three bands only the first two represent the intraligand π–π^* transition, and the third can be attributed to the intraligand n–π^* charge transfers.

There are three bands appearing in the spectrum of Cr(III) complex. The first band appeared at 220 nm, which represents the intraligand π–π^* transition. The second band appeared at 275 nm, which can be attributed to the intraligand n–π^* charge transfers. The third band, which is abroad band, appeared at range 435 nm, can be assigned to L → Cr(III) charge transfers. In the spectra of Fe(III) complex there are three bands, the first two represent the intraligand π–π^* transition, and the third can be attributed to the intraligand n–π^* charge transfers. The spectra of La(III) complex show four bands, the first two represent the intraligand π–π^* transition, and the second two can be attributed to the intraligand n–π^* charge transfers. The electronic spectrum of ZrO(II) complex is resample to the spectrum of Cr(III) complex but the two bands appeared at 245 and 285 nm.

There are five bands appearing in the spectrum of UO_2(II) complex. The first two band appeared at 225, 235 nm, which represented the intraligand π–π^* transition. The second two bands appeared at 245 and 280 nm, can be attributed to the intraligand n–π^* charge transfers. The fifth band, which is abroad band, appeared at range 400 nm, can be assigned to L → UO_2(II) charge transfers.

3.6. ^1H NMR spectra

The proton magnetic resonance spectra of the Sn(IV), Hg(II), Cr(III) and UO_2(II) complexes were analyzed in comparison of the spectra of the free ligand (Fig. 1). The ligand structure is shown in Scheme 2. The chemical shift (δ, ppm) of the different protons have been recorded in Table 5.

It is clear that all H protons (b–H, c–H, d–H and e–H) experience downfield shift in the L-tyrosine complex, except a–H has an up field shift, these data compared with free L-tyrosine ligand. Theoretically, the possible complex site were –NH_2, –OH and –COOH, but the chance of complex site of –OH with Sn(IV), Hg(II), Cr(III) and ZrO(II) elements is slim, only if the PH was very high in the system. In experimental section, the pH value was adjust at pH 7 (neutral).

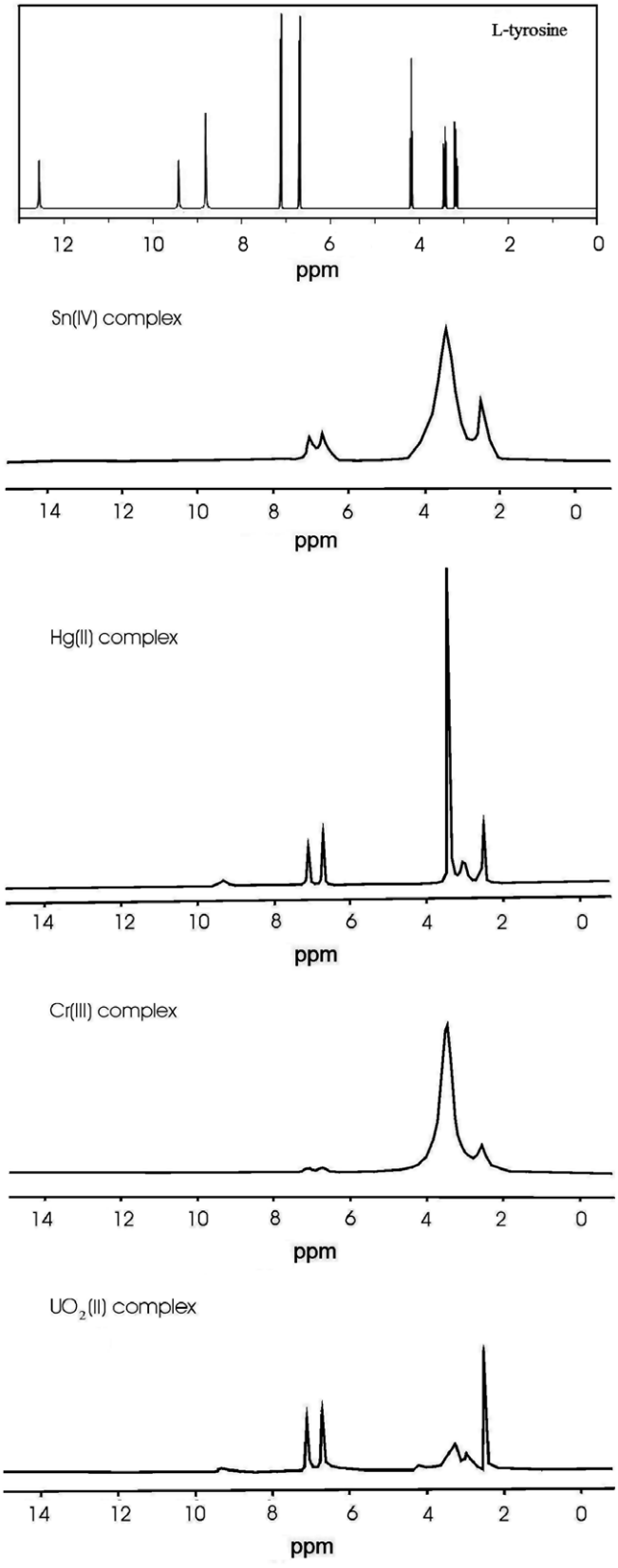

Fig. 1. The ^{1}H NMR spectra of L-tyrosine and its complexes.

Most amino acids are present as a single protonated from HL in the pH range 2.7–8.5. A few amino acids occur as H_2L, H_2L^+ from over the whole range. This is true for tyrosine where proton of phenolic group is not released. A comparison of metal–ligand stability constants values of tyrosine with those of serine permits the conclusion that the unionized hydroxyl group is not participating in the complex formation [31,32]. The coordination appears to be only through amino nitrogen and carboxylate oxygen.

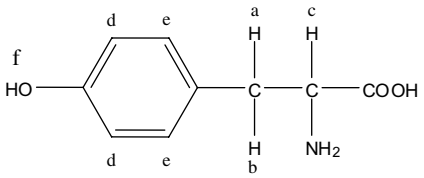

Scheme 2. Structure formula of L-tyrosine.

Table 5
The ^{1}H NMR spectral data[a] (δ, ppm)[b] of the ligand and its corresponding Sn(IV), Hg(II), Cr(III) and ZrO(II) complexes

Compound	a–H	b–H	c–H	d–H	e–H	f–H[c]
L-Tyrosine	2.61	2.72	3.33	6.50	6.85	9.83
$[Sn(tyr)_2(Cl)_2]$	2.50	–	3.39	6.68	7.04	10.80
$[Hg(tyr)_2]$	2.52	3.06	3.41	6.71	7.09	9.32
$[Cr(tyr)_3]\cdot 6H_2O$	2.58	–	3.50	6.77	7.07	9.50
$[UO_2(tyr)_2]$	2.49	2.93	3.26 4.20	6.71	7.11	9.35

[a] Solvent DMSO-d_6.
[b] Relative to TMS.
[c] The phenolic proton resonances not shifted indicating that (OH) group does not participate in bonding.

The brood signal exhibited by the ligand due to the OH (carboxylate group) proton at 12.34 ppm disappears in the tyrosine complexes indicating the coordination of oxygen atom (carboxylate ion) with the metal ion [33,34]. The appearance of signals due to (phenolic) protons of the same positions in the free ligand and in its complexes shows the non-involvement of this group in coordination.

Another fact is that the vibration of chemical shift of c–H is larger than a–H and b–H, indicating one of the complex sites was near to c–H, that is $–NH_2$.

3.7. Mass spectra

The electron impact mass spectrum of the free ligand (L-tyrosine) Fig. 2, confirm the proposed formula by showing a peak at $m/z = 181$ amu corresponding to L-tyrosine moiety [($C_9H_{11}NO_3$) atomic mass 181.19]. It also shows a series of peaks i.e. m/z (%)=136 (3.6), 107 (100), 76 (7.6) and 38 (2.4), corresponding to various fragments. This intensity gives an idea of stability of fragment. The fragmentation patterns of L-tyrosine are shown in Scheme 3.

The mass spectra of Sn(II), Zn(II), Fe(III) and UO_2(II) tyrosine are presented in Fig. 2. All of these complexes have two main molecular ion peaks, one of them concerning the molecular ion peak of tyrosine ion $m/z = 180$ amu (ligand) and the other important peak at $m/z = 118$, 65, 56 and 238 amu corresponding to the release of metal ions Sn(II), Zn(II), Fe(III) and UO_2(II), respectively.

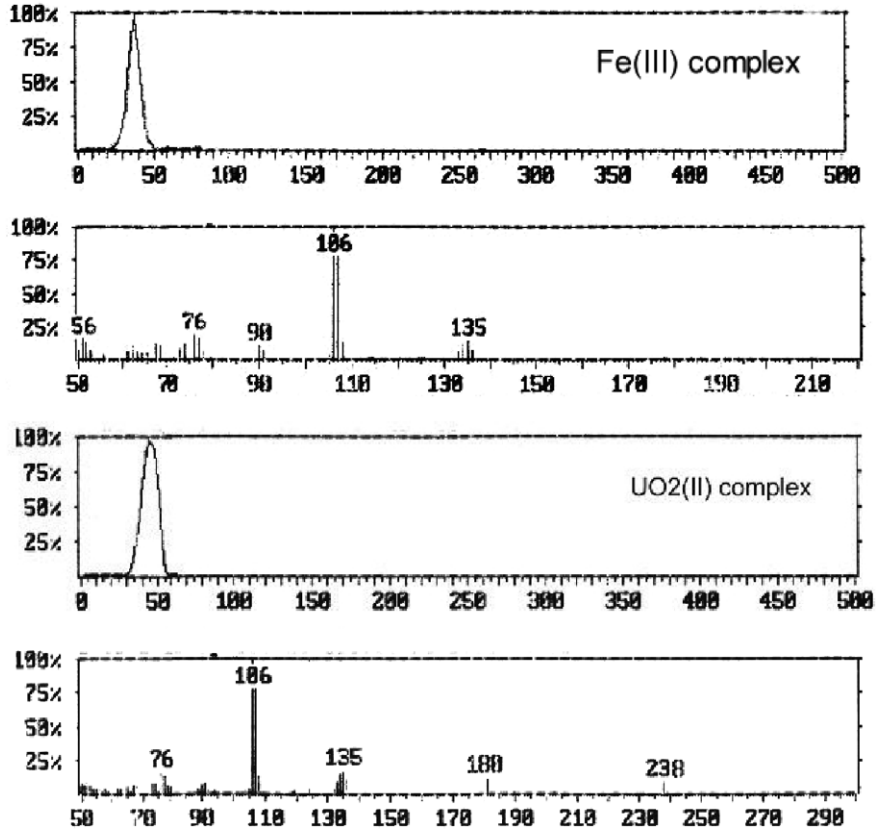

Fig. 2. The mass spectra L-tyrosine and its complexes.

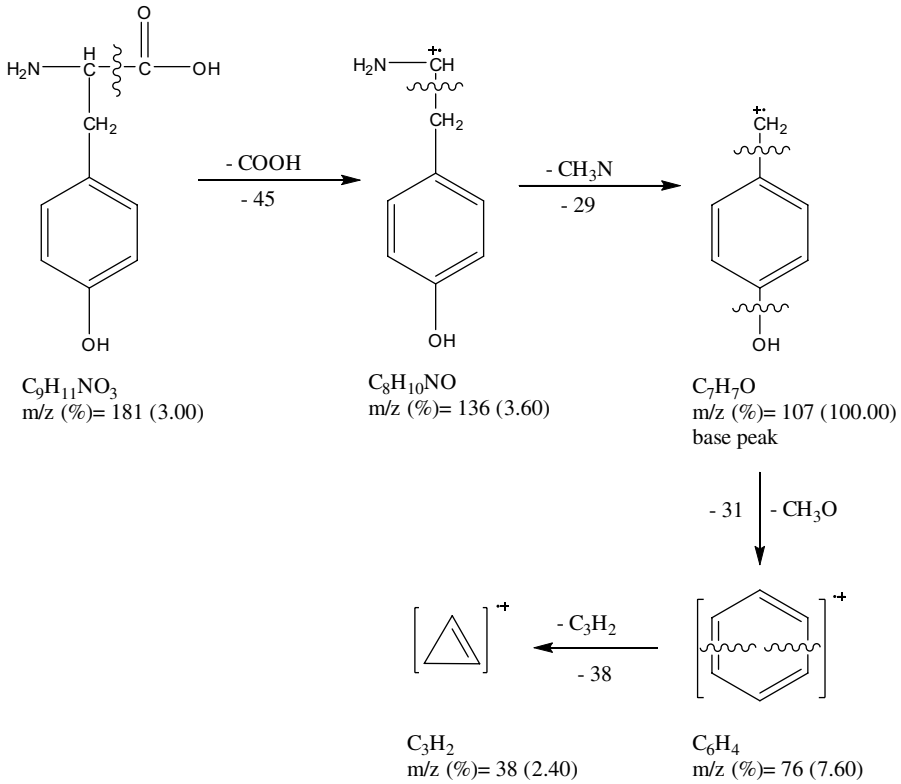

Scheme 3. Fragmentation scheme of L-tyrosine.

Both the L-tyrosinate complexes resulted herein and the L-tyrosine ligand show the base peaks at m/z 107, which due to the fragment, C_7H_7O. The data confirm the coordination mode of the metal tyrosinate complexes, this fact is greatly supported that, L-tyrosine act as bidentate ligand with coordination involving the carboxylic oxygen and the nitrogen atom of the amino group.

From the mass spectra (Fig. 2); the Sn(II)-tyrosinate complex possesses a series of peaks, i.e. $m/z = 180$, 135, 118, 106 and 77 amu corresponding to the release of $C_9H_{10}NO_3$, C_8H_9NO, Sn(II), C_7H_6O and C_6H_5; the Zn(II)-tyrosinate complex show the main fragment peaks at $m/z = 180$, 135, 106, 76 and 65 amu, which due to the fragments of $C_9H_{10}NO_3$, C_8H_9NO, C_7H_6O, C_6H_5 and Zn(II), respectively; the important fragments peaks of Fe(III)-tyrosinate complex at $m/z = 180$, 135, 106, 76 and 56 amu corresponding to the release of $C_9H_{10}NO_3$, C_8H_9NO, C_7H_6O, C_6H_5 and Fe(III), respectively; concerning, UO_2(II)-tyrosinate complex, the fragment patterns are observed at 238, 180, 135, 106 and 76 amu, which are due to the fragments: UO_2(II), $C_9H_{10}NO_3$, C_8H_9NO, C_7H_6O and C_6H_5, respectively.

From the two previously Schemes 4 and 5, can be concluded that:

(i) The present of the important fragment peak at $m/z = 135$ amu in all of our studied tyrosine complexes, proved that, the L-tyrosine ligand involved in the complexation as a tyrosinate feature.
(ii) The molecular ion peak, C_7H_6O $m/z = 106$ amu, which is exist in the tyrosinate complexes gives an interpretation about the non-participation of the phenolic group in the chelation between metal ions and L-tyrosine.
(iii) From the mass spectra (TLC) in the four fragment diagrams of Sn(II), Zn(II), Fe(III) and UO_2(II), it is clearly obvious that all of our studied tyrosinate complexes are pure and all of them have one peak.

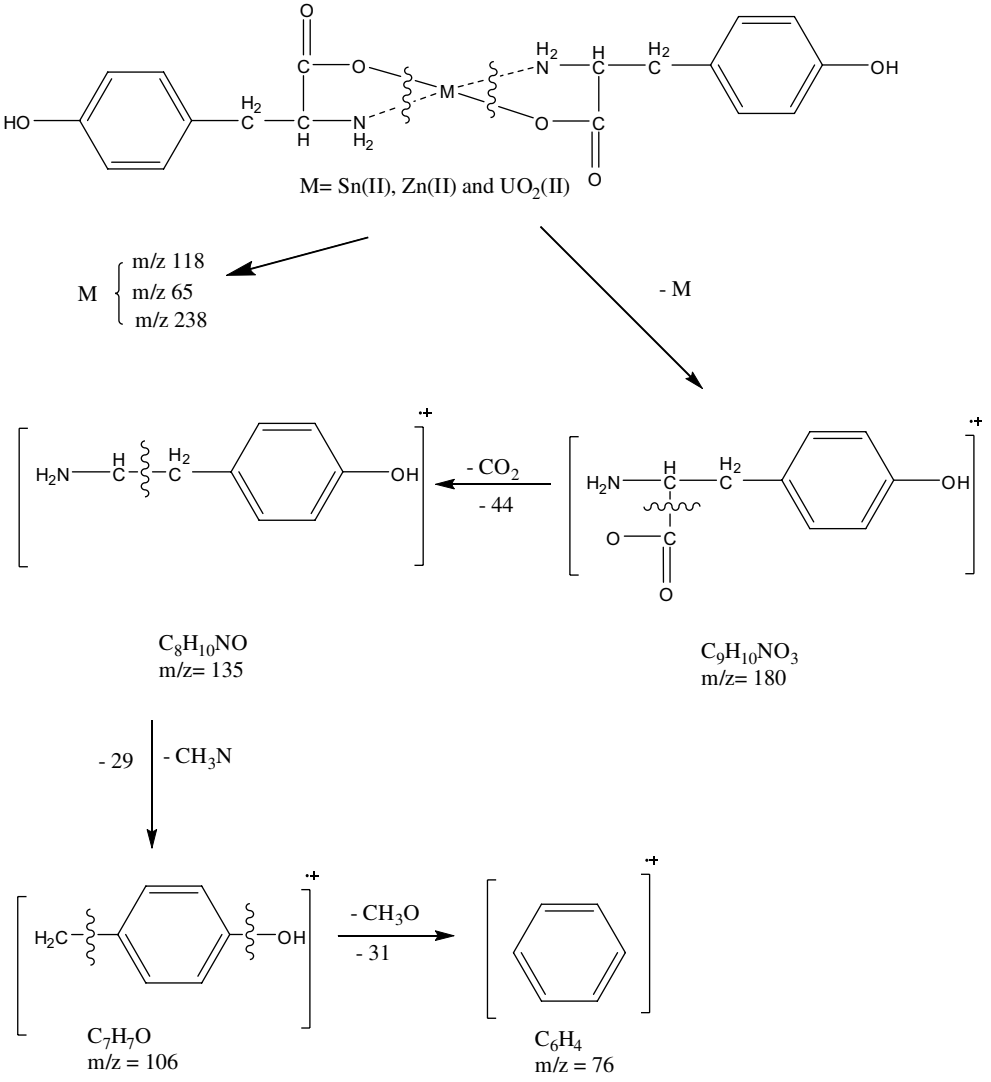

Scheme 4. Fragmentation scheme of Sn(II), Zn(II) and UO_2(II) tyrosinate complexes.

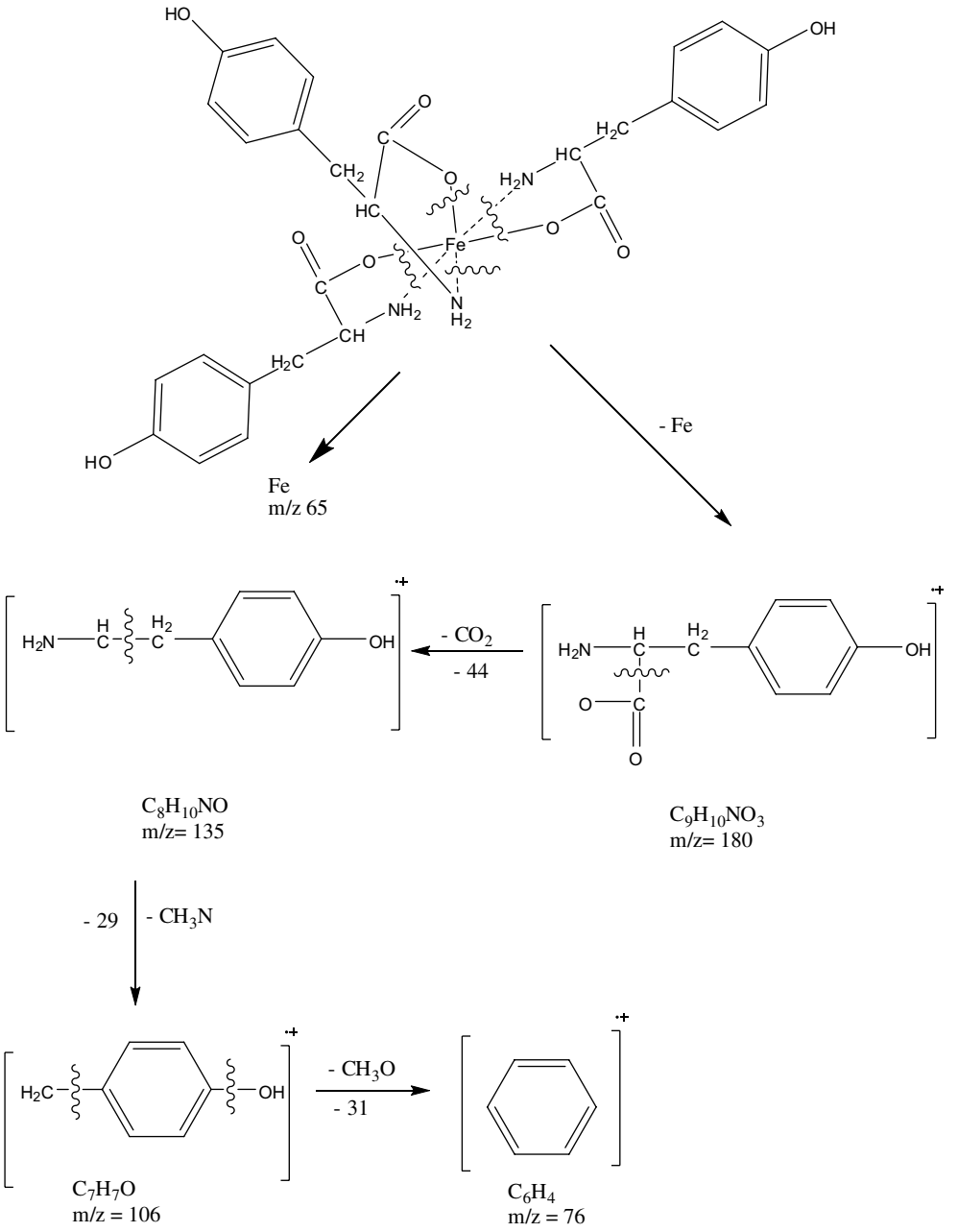

Scheme 5. Fragmentation scheme of Fe(III) tyrosinate complex.

3.8. Thermal analysis

Thermal techniques, such as thermogravimetric analysis (TGA and DTG), has been successfully employed for the study of the energetic of interactions of metal cations with biological species, such as amino acids [34,35]. The weight loss profiles are analyzed the amount or percent of weight loss at any given temperature, and the temperature ranges of the degradation process were determined [36].

Thermal stability domains, melting points, decomposition phenomena and their assignments for the L-tyrosinate complexes are summarized in Table 6. The simultaneous TG-DTG measurements of: L-tyr, $[Sn(tyr)_2]\cdot H_2O$, $[Sn(tyr)_2Cl_2]$, $[Zn(tyr)_2]\cdot 2H_2O$, $[Cd(tyr)_2]\cdot 2H_2O$, $[Hg(tyr)_2]$, $[Cr(tyr)_3]\cdot 6H_2O$, $[Fe(tyr)_3]$, $[La(tyr)_3]\cdot 7H_2O$, $[ZrO(tyr)_2]\cdot 2H_2O$ and $[UO_2(tyr)_2]$ compounds at the heating rate of 10 °C/min in the static nitrogen atmosphere were done.

The overall loss of mass from the TG curves is 67.08% for L-tyr, 63.37 for $[Sn(tyr)_2]\cdot H_2O$, 79.20% for $[Sn(tyr)_2Cl_2]$, 72.66% for $[Zn(tyr)_2]\cdot 2H_2O$, 74.70% for $[Cd(tyr)_2]\cdot 2H_2O$, 53.27% for $[Hg(tyr)_2]$, 53.41% for $[Cr(tyr)_3].6H_2O$, 78.58% for $[Fe(tyr)_3]$, 61.53% for $[La(tyr)_3]\cdot 7H_2O$, 74.04% for $[ZrO(tyr)_2]\cdot 2H_2O$ and 63.57% for $[UO_2(tyr)_2]$ compounds, respectively. All the complexes have two, three or four maxima peaks mass loss. The analysis of thermal curves of the complexes clearly indicates that the weight loss (first maximum peak) between 20 and 200 °C (except to $[La(tyr)_3]\cdot 7H_2O$ from 20 to 300 °C) corresponds to water

Table 6
Thermal data of L-tyrosine and its complexes

Compound	Steps	Temperature range (°C)	DTG peak (°C)		TG Weight loss (%)		Assignments
			Endo	Exo	Calc.	Found	
L-Tyr	1st	25–800	323	–	66.89	67.08	$-C_4H_{11}NO_3$ (organic moiety)
					33.11	32.92	5C (residue)
$[Sn(tyr)_2]\cdot H_2O$	1st	25–200	83	–	3.62	3.31	One mole of crystal water
	2nd	200–800	280	–	59.59	60.06	$C_{14}H_{20}N_2O_5$ (organic moiety)
					36.78	36.63	SnO + 4C (residue)
$[Sn(tyr)_2Cl_2]$	1st	25–300	276	–	38.93	38.45	$C_{14}H_{14}O_2$ (two, *p*-hydroxy phenyl)
	2nd	300–800	600	–	39.48	40.75	$C_4H_6N_2O_4Cl_2$(organic moiety)
					21.59	20.80	Sn (residue)
$[Zn(tyr)_2]\cdot 2H_2O$	1st	25–200	63	–	7.80	7.69	2 H_2O crystal water
	2nd	200–500	292	–	23.19	23.82	C_7H_7O (one, *p*-hydroxy phenyl)
	3rd	500–800	558	–	40.96	41.15	$C_7H_{13}N_2O_4$ (organic moiety)
					28.05	27.34	ZnO + 4C (residue)
$[Cd(tyr)_2]\cdot 2H_2O$	1st	25–220	217	–	7.08	6.88	2 H_2O crystal water
	2nd	220–250	238	–	21.05	20.64	C_7H_7O (one, *p*-hydroxy phenyl)
	3rd	250–350	301	–	21.05	20.64	C_7H_7O (one, *p*-hydroxy phenyl)
	4th	350–800	521	–	25.57	26.54	$C_4H_6N_2O_3$ (organic moiety)
					25.25	25.30	CdO (residue)
$[Hg(tyr)_2]$	1st	25–390	327	–	19.08	18.88	C_7H_7O (one, *p*-hydroxy phenyl)
	2nd	390–640	577	–	19.08	18.88	C_7H_7O (one, *p*-hydroxy phenyl)
	3rd	640–800	670	–	14.63	15.51	$H_6N_2O_3$
					47.21	46.73	HgO + 4C (residue)
$[Cr(tyr)_3]\cdot 6H_2O$	1st	25–200	101	–	15.44	16.32	6 H_2O crystal water
	2nd	200–340	276	–	15.29	14.84	C_7H_7O (one, *p*-hydroxy phenyl)
	3rd	340–800	506	–	24.14	22.25	$H_{23}N_3O_{6.5}$ (organic moiety)
					45.13	46.59	$1/2Cr_2O_3$ + 20C (residue)
$[Fe(tyr)_3]$	1st	25–500	264	–	53.85	53.71	$C_{21}H_{21}O_3$ (three, *p*-hydroxy phenyl)
	2nd	500–800	664	–	24.68	24.87	$C_2H_9N_3O_{4.5}$ (organic moiety)
					21.47	21.42	$1/2Fe_2O_3$ + 4C (residue)
$[La(tyr)_3]\cdot 7H_2O$	1st	25–300	275	–	15.64	15.58	7 H_2O
	2nd	300–800	475		46.25	45.95	$C_{15}H_{30}N_3O_{7.5}$ (organic moiety)
					38.11	38.47	$1/2La_2O_3$ + 12C (residue)
$[ZrO(tyr)_2]\cdot 2H_2O$	1st	25–200	117	–	7.15	6.53	2 H_2O
	2nd	200–800	306	–	68.37	67.51	$C_{18}H_{20}N_2O_5$ (organic moiety)
					24.48	25.96	ZrO_2 (residue)
$[UO_2(tyr)_2]$	1st	25–120	95	–	–	–	Melting point
	2nd	120–300	259	–	33.95	33.70	$C_{14}H_{14}O_2$ (two, *p*-hydroxy phenyl)
	3rd	300–800	–	660	28.29	29.87	$C_4H_6N_2O_6$ (organic moiety)
					37.76	36.43	Uranium metal (residue)

molecules for the hydrated complexes like, (Sn(II), Zn(II), Cd(II), Cr(III), La(III) and ZrO(II)). Because of the low temperatures, these water molecules may be considered as crystal water [37]. While the first (in case of non-hydrated complexes), second and third mass loss is due to the loss of one, two or three molecule of organic radicals (C_7H_7O-*p*-hydroxyphenyl) from contents of L-tyr ligand. The other decomposition peak was interpreted to the decomposition of the L-tyrosine rest. The end-products were confirmed with infrared spectra.

3.8.1. L-Tyrosine (ligand)

The 4-hydroxyphenylalanine (L-tyr) ligand melts at 343 °C with simultaneous decomposition. The main degradation peak was observed at 323 °C in the TG profile. From the TG profile of the L-tyr, it appears that the sample decomposes in one sharp stage over the wide temperature range 25–800 °C. The decomposition occurs with a mass loss of 67.08% and its calculated value is 66.89%.

3.8.2. $[Sn(tyr)_2]\cdot H_2O$ and $[Sn(tyr)_2Cl_2]$

Thermal analysis curves of the tin(II) and tin(IV) complexes show that decomposition takes places in two stages in temperature range 25–800 °C (DTG_{max}: 83 and 280 °C) for $[Sn(tyr)_2]\cdot H_2O$ complex and in between 25 and 800 °C (DTG_{max}: 276 and 600 °C) for $[Sn(tyr)_2Cl_2]$ complex. The two endothermic decomposition stages correspond to decomposition of the ligand. The TG curves of the two

complexes show a weight losses (found 63.37, calcd. 63.16% for Sn(II) complex and found 79.20, calcd. 78.41% for Sn(IV) complex) corresponding to the loss of (one crystal water molecule and organic moiety, $C_{14}H_{20}N_2O_5$) and (two *p*-hydroxyphenyl molecules, $C_{14}H_{14}O_2$ and organic moiety, $C_4H_6N_2O_4Cl_2$) for $[Sn(tyr)_2]\cdot H_2O$ and $[Sn(tyr)_2Cl_2]$ complexes, respectively. The final products, formed at 800 °C, consist of (SnO + 4C) and (Sn metal) for Sn(II) and Sn(IV) complexes, respectively. Reported data on thermal analysis studies were collected in nitrogen atmosphere media which, indicate that the two tin complexes decompose to give tin(II) oxide or tin metal (according to metal cations) and few carbon atoms as final products, interpretive for no sufficiently of oxygen atoms encouraged the liberated carbon as carbon monoxide or dioxide.

3.8.3. $[Zn(tyr)_2]\cdot 2H_2O$, $[Cd(tyr)_2]\cdot 2H_2O$ and $[Hg(tyr)_2]$

Thermal decomposition of d^{10} transition metals complexes; $[Zn(tyr)_2]\cdot 2H_2O$, $[Cd(tyr)_2]\cdot 2H_2O$ and $[Hg(tyr)_2]$ proceeds in three and/or four ranged main stages. These three-to-four stages are related to the decomposition of two hydrated water molecules and the organic part of the chelate like two molecule of organic radicals (C_7H_7O-*p*-hydroxyphenyl) from two molecules of the ligand and the following pyrolysis of the L-tyr rest; (found 72.66%; calcd. 71.95% for Zn(II) complex, found 74.70%; calcd. 74.75% for Cd(II) complex and found 53.27%; calcd. 52.79% for Hg(II) complex, respectively), in the temperature ranges 25–800 °C by giving an endothermic effect (DTG_{max}: 63, 292 and 558 °C; DTG_{max}: 217, 238, 301 and 521 °C and DTG_{max}: 327, 577 and 670 °C) for $[Zn(tyr)_2]\cdot 2H_2O$, $[Cd(tyr)_2]\cdot 2H_2O$ and $[Hg(tyr)_2]$ complexes, respectively. In the sequence stages, the Zn(II), Cd(II) and Hg(II) complexes decomposes in the final steps to oxide (MO; M = Zn, Cd and Hg).

3.8.4. $[Cr(tyr)_3]\cdot 6H_2O$, $[Fe(tyr)_3]$ and $[La(tyr)_3]\cdot 7H_2O$

The TG diagrams of $[Cr(tyr)_3]\cdot 6H_2O$, $[Fe(tyr)_3]$ and $[La(tyr)_3]\cdot 7H_2O$ complexes reveal mass loss in the temperature range 25–800 °C corresponding to the formation of $1/2M_2O_3$ (M = Cr, Fe and La). The two and/or three endothermic peaks were observed in DTG analysis. The maxims of these peaks are found to be (DTG_{max}; 101, 276 and 506 °C) for Cr(III) complex, (DTG_{max}; 264 and 664 °C) for Fe(III)-tyrosinate complex, (DTG_{max}; 275 and 475 °C), respectively. The first peak in case of chromium(III)-tyrosinate complex was discussed concerning to the loss of six uncoordinated water molecules of the Cr(III) complex. The Cr(III), Fe(III) and La(III) complexes are thermally stable up to 506, 664 and 475 °C, respectively. Respecting of Cr(III) complex, the second and third peaks correspond to decomposition of the ligand. The mass losses at 276 and 506 °C DTG_{max}, respectively, are endothermic decomposition and corresponding to the loss of one molecule of *p*-hydroxyphenyl moiety and $H_{23}N_3O_{6.5}$ organic rest, and then the final decomposition product is Cr_2O_3 (Fig. 3). The overall weight loss (found 53.41%, calcd. 54.87%) agrees well with the proposed structure. The Fe(III) and La(III)-tyrosinate complexes show a weight losses (found 78.58, calcd. 78.53% for Fe(III) complex and found 61.53, calcd. 61.89% for La(III) complex) corresponding to the loss of (three *p*-hydroxyphenyl molecules, $C_{21}H_{21}O_3$ and organic moiety, $C_2H_9N_3O_{4.5}$) and (seven water molecules and $C_{15}H_{30}N_3O_{7.5}$ as organic rest moiety) for $[Fe(tyr)_3]$ and $[La(tyr)_3]\cdot 7H_2O$ complexes, respectively. The final products, formed at 800 °C, consist of metal trioxide (Fig. 3).

3.8.5. $[ZrO(tyr)_2]\cdot 2H_2O$ and $[UO_2(tyr)_2]$

The TG of $[ZrO(tyr)_2]\cdot 2H_2O$ complex, two steps are shown in the pyrolysis curve at 117 and 306 °C. The first step corresponding to the dehydration of two water molecules (calcd.: 7.13%, found: 6.53%). The rest of the two tyrosinate molecules were decomposes in the last step with the formation of ZrO_2 as the final residue.

For UO_2(II)-tyrosinate complex consist of three decomposition steps at 95, 259 and 660 °C. The first step in the temperature range 25–120 °C corresponds to the melting point of the ligand, because no loss of weight was detected in the TG curve and the second step (DTG_{max}; 259 °C) seems to be consistent with evolution of two, *p*-hydroxy phenyl molecules (calcd.: 33.95%, found: 33.70%). It was hardly to detect the exact degradation of the organic moieties because of, this step is widely extending from 300 to

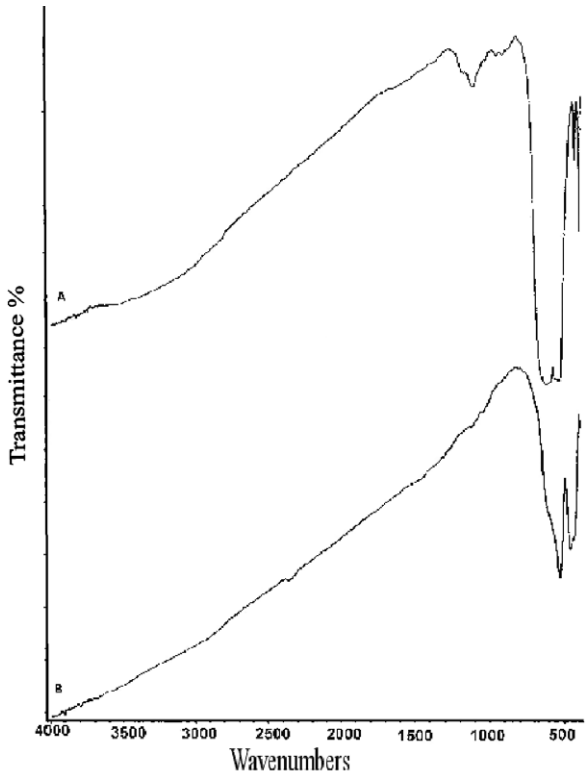

Fig. 3. The IR spectra of the metal trioxides; (a) Cr_2O_3 and (b) Fe_2O_3.

Table 7
Kinetic parameters determined using the Coats–Redfern (CR) and Horowitz–Metzger (HM) of the L-tyrosine and its complexes

Complex	Stage	Method	Parameter					r
			E (kJ mol^{-1})	A (s^{-1})	ΔS (J mol^{-1} K^{-1})	ΔH (kJ mol^{-1})	ΔG (kJ mol^{-1})	
L-Tyr	1st	CR	4.30×10^{5}	9.48×10^{35}	4.38×10^{2}	4.25×10^{5}	1.64×10^{5}	0.9997
		HM	4.39×10^{5}	1.19×10^{37}	4.59×10^{2}	4.35×10^{5}	1.61×10^{5}	0.9994
		Average	4.34×10^{5}	6.42×10^{36}	4.48×10^{2}	4.30×10^{5}	1.62×10^{5}	
I	1st	CR	3.13×10^{4}	6.89×10^{3}	-1.73×10^{2}	2.82×10^{4}	9.29×10^{4}	0.9954
		HM	3.84×10^{4}	1.98×10^{3}	-1.84×10^{2}	3.53×10^{4}	1.04×10^{5}	0.9952
			3.48×10^{4}	4.43×10^{3}	-1.78×10^{2}	3.17×10^{4}	9.84×10^{4}	
	2nd	CR	2.35×10^{5}	2.60×10^{20}	1.41×10^{2}	2.30×10^{5}	1.52×10^{5}	0.9921
		HM	2.39×10^{5}	8.12×10^{20}	1.50×10^{2}	2.34×10^{5}	1.51×10^{5}	0.9898
II	1st	CR	1.67×10^{5}	9.72×10^{13}	17.80	1.63×10^{5}	1.53×10^{5}	0.9973
		HM	1.74×10^{5}	6.52×10^{14}	33.60	1.69×10^{5}	1.51×10^{5}	0.9980
		Average	1.70×10^{5}	3.74×10^{3}	25.70	1.66×10^{5}	1.52×10^{5}	
	2nd	CR	2.17×10^{5}	4.66×10^{10}	−49.60	2.09×10^{5}	2.53×10^{5}	0.9968
		HM	2.30×10^{5}	4.94×10^{10}	−30.00	2.22×10^{5}	2.49×10^{5}	0.9955
		Average	2.23×10^{5}	4.60×10^{10}	−39.80	2.15×10^{5}	2.51×10^{5}	
III	1st	CR	1.49×10^{5}	2.63×10^{21}	1.64×10^{2}	1.46×10^{5}	9.06×10^{4}	0.9939
		HM	1.54×10^{5}	3.91×10^{21}	1.87×10^{2}	1.52×10^{5}	8.88×10^{4}	0.9916
		Average	1.51×10^{5}	3.27×10^{21}	1.75×10^{2}	1.48×10^{5}	8.97×10^{4}	
	2nd	CR	1.97×10^{5}	5.08×10^{15}	50.50	1.92×10^{5}	1.64×10^{5}	0.9635
		HM	2.06×10^{5}	2.73×10^{17}	83.60	2.02×10^{5}	1.55×10^{5}	0.9659
		Average	2.02×10^{5}	1.39×10^{17}	67.05	1.97×10^{5}	1.59×10^{5}	
	3rd	CR	1.31×10^{5}	4.32×10^{5}	-1.46×10^{2}	1.24×10^{5}	2.45×10^{5}	0.9811
		HM	1.42×10^{5}	5.57×10^{5}	-1.24×10^{2}	1.36×10^{5}	2.39×10^{5}	0.9785
		Average	1.36×10^{5}	1.94×10^{5}	-1.81×10^{2}	1.30×10^{5}	2.69×10^{5}	
IV	1st	CR	3.36×10^{4}	2.30×10^{3}	-1.82×10^{2}	3.07×10^{4}	9.40×10^{4}	0.9904
		HM	4.20×10^{4}	2.07×10^{3}	-1.64×10^{2}	3.91×10^{4}	9.60×10^{4}	0.9942
		Average	3.78×10^{4}	2.05×10^{3}	-1.73×10^{2}	3.49×10^{4}	9.50×10^{4}	
	2nd	CR	2.76×10^{5}	3.03×10^{27}	2.77×10^{2}	2.72×10^{5}	1.36×10^{5}	0.9972
		HM	2.80×10^{5}	2.19×10^{28}	2.94×10^{2}	2.76×10^{5}	1.32×10^{5}	0.9991
		Average	2.78×10^{5}	1.24×10^{5}	2.85×10^{2}	2.74×10^{5}	1.34×10^{5}	
	3rd	CR	2.52×10^{5}	4.99×10^{23}	2.04×10^{2}	2.47×10^{5}	1.43×10^{5}	0.9892
		HM	2.48×10^{5}	6.83×10^{23}	2.07×10^{2}	2.44×10^{5}	1.38×10^{5}	0.9843
		Average	2.50×10^{5}	5.91×10^{23}	2.05×10^{5}	2.45×10^{5}	1.40×10^{5}	
	4th	CR	2.08×10^{5}	2.35×10^{17}	82.20	2.03×10^{5}	1.56×10^{5}	0.9978
		HM	2.29×10^{5}	1.48×10^{19}	117.0	2.24×10^{5}	1.57×10^{5}	0.9964
		Average	2.18×10^{5}	7.51×10^{18}	99.0	2.13×10^{5}	1.56×10^{5}	
V	1st	CR	2.21×10^{5}	1.84×10^{17}	79.8	2.16×10^{5}	1.68×10^{5}	0.9955
		HM	2.40×10^{5}	1.57×10^{19}	117.0	2.35×10^{5}	1.65×10^{5}	0.9960
		Average	2.61×10^{5}	4.94×10^{18}	98.4	2.25×10^{5}	1.65×10^{5}	
	2nd	CR	1.28×10^{5}	2.49×10^{7}	−110.0	1.22×10^{5}	1.97×10^{5}	0.9840
		HM	1.33×10^{5}	1.56×10^{8}	−94.9	1.27×10^{5}	1.92×10^{5}	0.9816
		Average	1.30×10^{5}	9.04×10^{7}	−102.4	1.25×10^{5}	1.95×10^{5}	
	3rd	CR	4.94×10^{5}	2.63×10^{28}	2.90×10^{2}	4.86×10^{5}	2.40×10^{5}	0.9879
		HM	5.08×10^{5}	3.88×10^{29}	3.13×10^{2}	5.01×10^{5}	2.36×10^{5}	0.9874
		Average	5.01×10^{5}	2.07×10^{29}	3.01×10^{2}	5.43×10^{5}	2.38×10^{5}	
VI	1st	CR	4.11×10^{4}	3.00×10^{3}	−180.0	3.80×10^{4}	1.05×10^{5}	0.9921
		HM	9.28×10^{4}	1.97×10^{11}	−30.6	8.97×10^{4}	1.01×10^{5}	0.9960
		Average	6.69×10^{4}	9.85×10^{10}	−105.3	6.38×10^{4}	1.03×10^{5}	
	2nd	CR	1.74×10^{5}	6.12×10^{14}	33.10	1.70×10^{5}	1.52×10^{5}	0.9980
		HM	1.85×10^{5}	7.53×10^{15}	54.00	1.80×10^{5}	1.51×10^{5}	0.9995
		Average	1.79×10^{5}	4.07×10^{15}	43.55	1.75×10^{5}	1.51×10^{5}	
	3rd	CR	9.33×10^{4}	3.40×10^{5}	-1.45×10^{2}	8.81×10^{4}	1.79×10^{5}	0.9882
		HM	1.04×10^{5}	4.00×10^{5}	-1.25×10^{2}	9.91×10^{4}	1.77×10^{5}	0.9995
		Average	9.86×10^{4}	3.70×10^{5}	-1.35×10^{2}	9.36×10^{4}	1.78×10^{5}	
VII	1st	CR	2.08×10^{5}	3.01×10^{18}	1.04×10^{2}	2.04×10^{5}	1.48×10^{5}	0.9978
		HM	2.22×10^{5}	7.70×10^{19}	1.31×10^{2}	2.17×10^{5}	1.47×10^{5}	0.9985
		Average	2.15×10^{5}	4.00×10^{19}	1.17×10^{2}	2.10×10^{5}	1.47×10^{5}	
	2nd	CR	9.52×10^{4}	3.22×10^{4}	-1.86×10^{2}	8.86×10^{4}	2.37×10^{5}	0.9798
		HM	1.02×10^{5}	2.46×10^{4}	-1.69×10^{2}	9.58×10^{4}	2.31×10^{5}	0.9802
		Average	9.86×10^{4}	2.84×10^{4}	-1.77×10^{2}	9.22×10^{4}	2.34×10^{5}	

(*continued on next page*)

Table 7 (*continued*)

Complex	Stage	Method	Parameter					r
			E (kJ mol^{-1})	A (s^{-1})	ΔS (J mol^{-1} K^{-1})	ΔH (kJ mol^{-1})	ΔG (kJ mol^{-1})	
VIII	1st	CR	3.31×10^{4}	2.08×10^{3}	-1.83×10^{2}	3.02×10^{4}	9.38×10^{4}	0.9860
		HM	3.95×10^{4}	8.28×10^{3}	-1.71×10^{2}	3.66×10^{4}	9.62×10^{4}	0.9950
		Average	3.63×10^{4}	5.18×10^{3}	-1.77×10^{2}	3.34×10^{4}	9.50×10^{4}	
	2nd	CR	2.22×10^{5}	1.85×10^{19}	1.19×10^{2}	2.17×10^{5}	1.52×10^{5}	0.9943
		HM	2.28×10^{5}	1.28×10^{19}	1.35×10^{2}	2.24×10^{5}	1.50×10^{5}	0.9931
		Average	2.25×10^{5}	1.56×10^{19}	1.27×10^{2}	2.20×10^{5}	1.51×10^{5}	
IX	1st	CR	3.10×10^{4}	9.33×10^{3}	-1.71×10^{2}	2.78×10^{4}	9.44×10^{4}	0.9708
		HM	3.54×10^{4}	3.94×10^{2}	-1.97×10^{2}	3.21×10^{4}	1.09×10^{5}	0.9782
		Average	3.32×10^{4}	4.86×10^{3}	-1.84×10^{2}	2.99×10^{4}	1.01×10^{5}	
	2nd	CR	2.97×10^{5}	1.00×10^{25}	2.28×10^{2}	2.92×10^{5}	1.60×10^{5}	0.9994
		HM	3.09×10^{5}	1.96×10^{25}	2.53×10^{2}	3.04×10^{5}	1.58×10^{5}	0.9995
		Average	3.03×10^{5}	1.98×10^{25}	2.40×10^{2}	2.98×10^{5}	1.59×10^{5}	
X	1st	CR	1.46×10^{5}	1.57×10^{19}	1.21×10^{2}	1.43×10^{5}	9.83×10^{4}	0.9954
		HM	1.53×10^{5}	1.56×10^{19}	1.40×10^{2}	1.50×10^{5}	9.81×10^{4}	0.9929
		Average	1.49×10^{5}	1.56×10^{19}	1.30×10^{2}	1.46×10^{5}	9.82×10^{4}	
	2nd	CR	2.75×10^{5}	2.24×10^{25}	2.36×10^{2}	2.71×10^{5}	1.46×10^{5}	0.9880
		HM	2.87×10^{5}	4.64×10^{25}	2.61×10^{2}	2.83×10^{5}	1.44×10^{5}	0.9896
		Average	2.81×10^{5}	6.88×10^{25}	2.48×10^{2}	2.76×10^{5}	1.45×10^{5}	
	3rd	CR	1.14×10^{5}	4.82×10^{7}	-1.24×10^{2}	1.08×10^{5}	1.91×10^{5}	0.9770
		HM	1.23×10^{5}	2.78×10^{7}	-1.09×10^{2}	1.17×10^{5}	1.91×10^{5}	0.9739
		Average	1.18×10^{5}	3.80×10^{6}	-1.16×10^{2}	1.12×10^{5}	1.91×10^{5}	

800 °C. The weight loss of this complex is 29.87% and its calculated value is 28.29%.

3.9. Kinetic studies

In recent years there has been increasing interest in determining the rate-dependent parameters of solid-state non-isothermal decomposition reactions by analysis of TG curves. Several equations [38–45] have been proposed as means of analyzing a TG curve and obtaining values for kinetic parameters. Many authors [38–42] have discussed the advantages of this method over the conventional isothermal method. The rate of a decomposition process can be described as the product of two separate functions of temperature and conversion [39], using

$$d\alpha/dt = k(T)f(\alpha) \quad (1)$$

where α is the fraction decomposed at time t, $k(T)$ is the temperature dependent function and $f(\alpha)$ is the conversion function dependent on the mechanism of decomposition. It has been established that the temperature dependent function $k(T)$ is of the Arrhenius type and can be considered as the rate constant k.

$$k = Ae^{-E^*/RT} \quad (2)$$

where R is the gas constant in (J mol^{-1} K^{-1}). Substituting Eq. (2) into Eq. (1), we get,

$$d\alpha/dT = (A/\phi e^{-E^*/RT})f(\alpha)$$

where ϕ is the linear heating rate dT/dt. On integration and approximation, this equation can be obtained in the following form

$$\ln g(\alpha) = -E^*/RT + \ln[AR/\phi E^*]$$

where $g(\alpha)$ is a function of α dependent on the mechanism of the reaction. The integral on the right-hand side is known as temperature integral and has no closed for solution. So, several techniques have been used for the evaluation of temperature integral. Most commonly used methods for this purpose are the differential method of Freeman and Carroll [38] integral method of Coat and Redfern [40], the approximation method of Horowitz and Metzger [43].

In the present investigation, the general thermal behaviors of the L-tyrosine ligand and the 10 complexes in terms of stability ranges, peak temperatures and values of kinetic parameters are tabulated Table 7. The kinetic parameters have been evaluated using the following methods and the results obtained by these methods are compared with one another. The following two methods are discussed in brief.

3.9.1. Coats–Redfern equation

The Coats–Redfern equation, which is a typical integral method, can be represented as:

$$\int_0^{\alpha} \frac{d\alpha}{(1-\alpha)^n} = \frac{A}{\varphi}\int_{T_1}^{T_2} \exp\left(-\frac{E^*}{RT}\right)dt$$

For convenience of integration the lower limit T_1 is usually taken as zero. This equation on integration gives;

$$\ln\left[-\frac{\ln(1-\alpha)}{T^2}\right] = -\frac{E^*}{RT} + \ln\left[\frac{AR}{\varphi E^*}\right]$$

A plot of left-hand side (LHS) against $1/T$ was drawn. E^* is the energy of activation in kJ mol^{-1} and calculated from the slop and A in (s^{-1}) from the intercept value. The entropy of activation ΔS^* in (J K^{-1} mol^{-1}) was calculated by using the equation:

Table 8
Antibacterial activity data of the L-tyrosine and its complexes

Compound	*Bacillus subtilis*	*Serratia*	*Pseudomonas aeruginosa*	*E. coli*
L-Tyrosine	+++	–	+++	++++
$[Sn(tyr)_2]\cdot H_2O$	+++	–	++	+
$[Sn(tyr)_2(Cl)_2]$	++++	–	+++	++
$[Zn(tyr)_2]\cdot 2H_2O$	+++	++++	++++	++
$[Cd(tyr)_2]\cdot 2H_2O$	+++	–	+	+++
$[Hg(tyr)_2]$	+++	++++	++	++++
$[Cr(tyr)_3]\cdot 6H_2O$	++++	–	+++	–
$[Fe(tyr)_3]$	++++	–	+++	++
$[La(tyr)_3]\cdot 7H_2O$	++++	–	++	–
$[ZrO(tyr)_2]\cdot 2H_2O$	–	–	–	++
$[UO_2(tyr)_2]$	+	–	–	+++

(–) NO antibacterial activity, (+) mild activity, (++) moderate activity, (+++) marked activity, (++++) strong marked activity.

$$\Delta S^* = R\ln(Ah/k_B T_s) \quad (3)$$

where k_B is the Boltzmann constant, h is the Plank's constant and T_s is the DTG peak temperature [46].

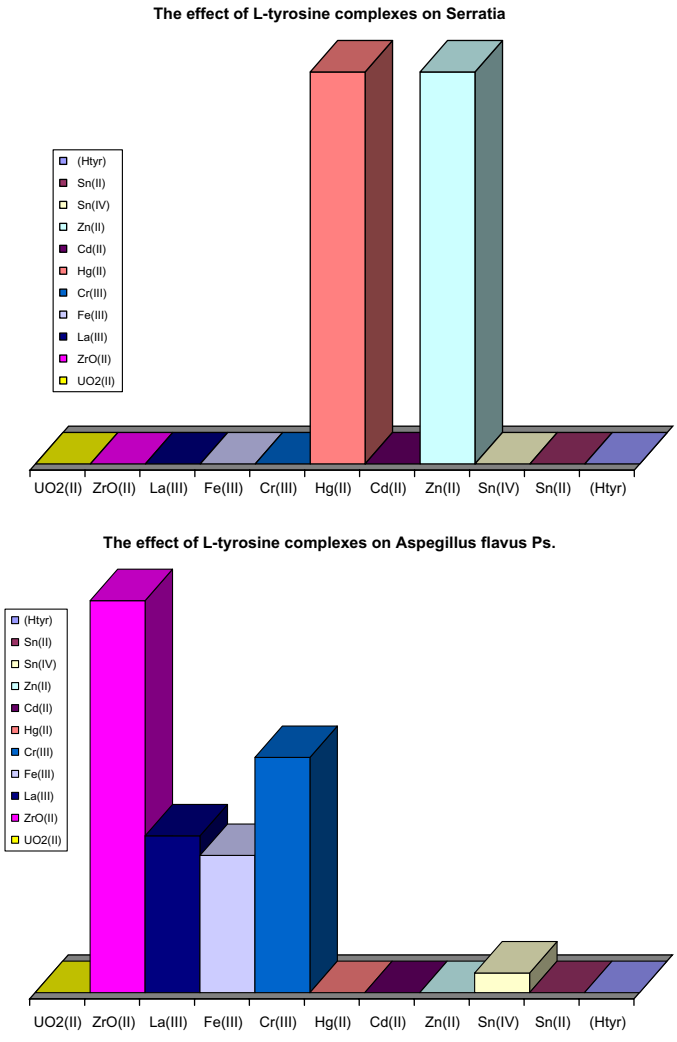

Fig. 4. The inhabitation zone of the L-tyrosine and their metal complexes on some kinds of bacterial and fungi.

3.9.2. Horowitz–Metzger equation

The Horowitz–Metzger equation is an illustrative of the approximation methods. These authors derived the relation:

$$log[\{1-(1-\alpha)^{1-n}\}/(1-n)] = E^*\theta/2.303RT_s^2 \quad \text{for} \quad n \neq 1 \quad (4)$$

When $n = 1$, the LHS of Eq. (4) would be $\log[-\log(1-\alpha)]$. For a first-order kinetic process the Horowitz–Metzger equation may be written in the form:

$$\log[\log(w_\alpha/w_\gamma)] = E^*\theta/2.303RT_s^2 - \log 2.303$$

where $\theta = T - T_s$, $w_\gamma = w_\alpha - w$, w_α = mass loss at the completion of the reaction; w = mass loss up to time t. The plot of $\log[\log(w_\alpha/w_\gamma)]$ vs θ was drawn and found to be linear from the slope of which E^* was calculated. The pre-exponential factor, A, was calculated from the equation:

$$E^*/RT_s^2 = A/[\phi\exp(-E^*/RT_s)]$$

The entropy of activation, ΔS^*, was calculated from Eq. (3). The enthalpy activation, ΔH^*, and Gibbs free energy, ΔG^*, were calculated from; $\Delta H^* = E^* - RT$ and $\Delta G^* = \Delta H^* - T\Delta S^*$, respectively.

Table 9
Antifungal activity data for L-tyrosine and its complexes

Compound	*Aspergillus flavus*	*Fusarium solani*	*Penicillium verrucosum*
L-Tyrosine	–	–	+
$[Sn(tyr)_2]\cdot H_2O$	–	–	–
$[Sn(tyr)_2(Cl)_2]$	+	–	+
$[Zn(tyr)_2]\cdot 2H_2O$	–	+++	+
$[Cd(tyr)_2]\cdot 2H_2O$	–	+	–
$[Hg(tyr)_2]$	–	+	+
$[Cr(tyr)_3]\cdot 6H_2O$	+++	++++	+
$[Fe(tyr)_3]$	++	++++	+
$[La(tyr)_3]\cdot 2H_2O$	++	+++	+
$[ZrO(tyr)_2]\cdot 2H_2O$	++++	++	++
$[UO_2(tyr)_2]$	–	++	+

(–) NO antibacterial activity, (+) mild activity, (++) moderate activity, (+++) marked activity, (++++) strong marked activity.

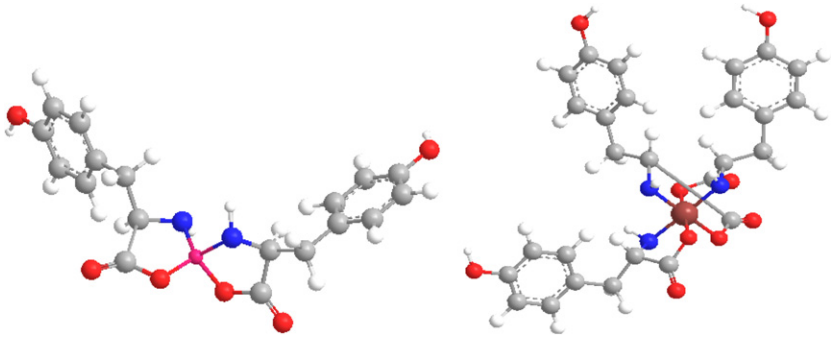

Scheme 6. The structures of di-, tri-, and tetra-valent metal ion complexes.

3.10. Microbiological investigation

L-Tyrosine is sometimes recommended by practitioners as helpful for weight loss, clinical depression, Parkinson's disease, and phenyl ketonuria; however, one study found that it had no impact on endurance exercise performance. It is useful in phenyl ketonuria because whereas phenyl ketonurias cannot met a bolize phenylalanine into tyrosine, they just stay off the phenylalanine and set treated with tyrosine and other amino acids extracted from proteins [47].

The results of antibacterial actives in vitro of the ligand and the complexes are shown in Table 8 and Fig. 4. From the results we can see that all the test compounds have lower antibacterial on *Serratia* (except for Zn(II) and Hg(II) tyrosinate complexes) and the (Sn(IV), Cr(III), Fe(III) and La(III) tyrosinate complexes) enhanced the activity on *Bacillus subtilis*. The zinc(II) tyrosinate complex has high activity against *Pseudomonas aeruginosa*. The L-tyrosine and their complexes have been evaluated for their antifungal activity. The minimal inhibitory concentration values listed in Table 9 show that all the test compounds have the order of antifungal activity as *Fusarium solani* > *Aspergillus flavus* > *Penicillium verrucosum*.

3.11. Structure of the tyrosinate complexes

The structures of the L-tyrosinate complexes (I–X) accordingly the above interpretation using elemental analysis, magnetic studies, molar conductance, (infrared, ^{1}H NMR, Mass) spectra as well as thermogravimetric analysis can be suggested as shown in Scheme 6.

References

[1] Norbert sewald and Hans-Dieter jakube "peptides: chemistry and biology, wiley-VCH verlag Gmb H& Co. KGaA, 2002.
[2] passim J.P. Greenstein, M. Winitz, Chemistry of the Amino Acids, vol. 1–3, John Wiley and Sons, Inc., New York, 1961.
[3] A. Magnuson, Y. Frapart, M. Abrahamsson, O. Horner, B. Kermark, L. Sun, G. Jean-Jacques, L. Hammarstroem, S. Styring, J. Am. Chem. Soc. 121 (1) (1999) 89.
[4] R.J.W. Hefford, L.D. Pettit, J. Chem. Soc. Dalton Trans. (1981) 1331.
[5] D. Van der Helm, C.E. Tatsch, Acta Crystallogr. Sect. B 28 (1972) 2307.
[6] B.L. Vallee, W.E.C. Wacker, in: H. Neurath (Ed.), Metalloproteins, vol. 5, Academic Press, New York and London, 1970.
[7] T. Kiss, A. Gergely, J. Chem. Soc. Dalton Trans. (1984) 1951.
[8] J.E. Letter Jr, J.E. Bauman Jr, J. Am. Chem. Soc. 92 (1970) 443.
[9] Hao Xu, Liang Chen, Spectrochim. Acta A 59 (2003) 657.
[10] G. Devi Indira, Parameswaran Geetha, S.S. Veena, Asian J. Chem. 16 (2) (2004) 884.
[11] C.A. McAuliffe, S.G. Murray, Inorgan. Chim. Acta 7 (1973) 171.
[12] (a) S.H. Lauri, Chem. Comm. 155 (1967);
(b) Aust. J. Chem. 20 (1967) 2609.
[13] A. Earnshow, Introduction to Magneto Chemistry, Academic press, New York, 1968.
[14] W.J. Geary, Coord. Chem. Rev. 7 (1971) 81.
[15] K. Nakamoto, Infrared and Raman Spectra of Inorganic and Coordination compounds, fourth ed., Wiley, New York, 1986.
[16] Y. Inomata, T. Inomata, T. Moriwaki, Bull. Chem., Soc. Jap. 47 (4) (1974) 818.
[17] J.F. Vilia, W.E. Hatfield, Chem. Phys. Lett. 9 (6) (1971) 568.
[18] T.J. Lane, J.A. Durkin, R.J. Hooper, Spectrochim. Acta 20 (1964) 1017.
[19] I. Nakagaw, R.J. Hooper, J.L. Walter, T.J. Lane, Spectrochim. Acta 21 (1965) 1.
[20] J.F. Jackovitz, J.L. Walter, Spectrochim. Acta 22 (1966) 1393.
[21] J.F. Jackovitz, J.A. Durkin, J.L. Walter, Spectrochim. Acta 23A (1967) 67.
[22] R.F. de farieas, J. Scatena Jr., C. Airoldi, J. Inorg. Biochem. 73 (1999) 253.
[23] R.F. de farieas, C. Airoldi, J. Inorg. Biochem. 76 (1999) 273.
[24] S.P. Mc Glynm, J.K. Smish, W.C. Neely, J. Chem. Phys. 35 (1961) 105.
[25] L.H. Jones, Spectrochim. Acta 15 (1959) 409.
[26] J. Selbin, Chem. Rev. 65 (1965) 153.
[27] W. Barnum, J. Inorg. Nucl. Chem. 21 (1961) 221.
[28] R.H. Holm, F.A. Cotton, J. Am. Chem. Soc. 80 (1958) 5658.
[29] F.A. Cotton, C.W. Wilkinson, in: Advanced Inorganic Chemistry, third ed., Interscience Publisher, New York, 1972.
[30] J.E. Letter Jr., J.E. Bauman Jr., J. Am. Chem. Soc. 92 (1970) 447.
[31] V.D. Panasynk, V.A. Golab, Russ. J. Inorg. Chem. 14 (1965) 1485.
[32] R. Roy, M.C. Saha, P.S. Roy, Trans. Met. Chem. 5110 (1990) 51.
[33] P.P. Carbi, F. Cagnim, L.P.B. Sabeh, A.C. Massabni, C.M. Costa-Neto, Spectrochim. Acta part A 66 (4–5) (2007) 1171.
[34] R.F. de Farias, H.C. Airoldi, H. Scatena Jr., J. Inorg. Biochem. 73 (1999) 253.
[35] R.F. de Farias, H.C. Airoldi, J. Inorg. Biochem. 76 (1999) 273.
[36] K. Burger, Coordination Chemistry: Experimental Methods, Akademiai Kiado, Budapest, 1973, p. 23.
[37] Qu Lunyu, Sun Yingji, Chen Yaguang, Yu Ming, Pen Jun, Synth. React. Inorg. Met.-Org. Chem. 24 (1994) 1339.
[38] E.S. Freeman, B. Carroll, J. Phys. Chem. 62 (1958) 394.

[39] J. Sestak, V. Satava, W.W. Wendlandt, Thermochim. Acta 7 (1973) 333.
[40] A.W. Coats, J.P. Redfern, Nature 201 (1964) 68.
[41] T. Ozawa, Bull. Chem. Sot. Jpn. 38 (1965) 1881.
[42] W.W. Wendlandt, Thermal Methods of Analysis, Wiley, New York, 1974.
[43] H.W. Horowitz, G. Metzger, Anal. Chem. 35 (1963) 1464.
[44] J.H. Flynn, L.A. Wall, Polym. Lett. 4 (1966) 323.
[45] P. Kofstad, Nature 179 (1957) 1362.
[46] J.H.F. Flynn, L.A. Wall, J. Res. Natl. Bur. Stand. 70A (1996) 487.
[47] A.C. par cell et al., J. Appl. Physiol. 93 (5) (2002) 1590.